NUMERICAL INVESTIGATION OF THE FLOW FIELD OF A CONFINED TURBULENT IMPINGING JET

Latifa Rezg and Dinh Vo-Ngoc
Department of Mechanical Engineering
École de Génie
Université de Moncton
Moncton E1A 3E9, CANADA

ABSTRACT

The paper presents results of numerical simulation, using a control volume based finite difference method, of the flow-field due to an axial turbulent impinging jet into parallel discs. Both high-Reynolds and low-Reynolds number (Launder-Sharma) versions of k-ε turbulence models were used. The parameters studied were the jet Reynolds number ($4000<Re<23000$) and nozzle-to-impingement surface spacing ($1<H/D<4$). The low-Reynolds model presented by Launder-Sharma shows better agreements with the experimental data of *Fitzgerald and Garimella (1998)* for mean velocity profiles. Discrepancy over turbulence intensity is obvious as obtained by *Craft et al (1993)* in the case of unconfined jet using same turbulence models.

INTRODUCTION

Impinging jets are used in a wide variety of applications, where high rates of heat and mass transfer are desired. Practical applications include for example cooling of turbine blades and electrical equipment, drying of paper and textiles. Extensive literature on heat and mass transfer characteristics under unconfined jets are available (*Jambunathan et al (1992)* and *Jambunathan and Button (1994)*). However limited works on the effect of confinement in jet impingement have been reported, and especially when the flow is confined between two parallel discs. In the case of planar jet, the effect of confinement on the flow field and heat transfer has been done numerically by *Seyedein et al (1994)*. They have investigated the effectiveness of various two-equation k-ε models for modelling the turbulent confined jet flow. They have shown that the standard k-ε turbulence model is not the best model for simulating the confined turbulent impinging jet and requires the use of new model for the near wall layer viscous effects; while the low Reynolds k-ε model proposed by *Launder and Sharma (1974)(LS)* gave results in good agreement with experiments. Furthermore, *Barata et al (1991)* presented their findings that the k-ε model is useful for the prediction of the mean flow field for a single and twin planar jets. Nevertheless, for submerged and confined axisymmetric jet, very rare information is available numerically for the turbulent case. Recently, flow field measurements have been made at the impingement section for submerged and confined axisymmetric liquid jet by *Fitzgerald and Garimella (1998)*. They have shown a toroidal recirculation pattern, which is characteristic of confined jets. The recirculation zone moves radially outward, both with increasing the Reynolds number and the spacing between nozzle to target plate.

The objective of the present study is to investigate numerically the characteristics of the flow field of an axisymmetric confined jet by using the LS version of the low-Reynolds number model as well as the standard k-ε model. Numerical results are compared to those of the experimental data of *Fitzgerald and Garimella (1998)*.

MATHEMATICAL FORMULATION

1) Turbulence model

In the present study, the flow is assumed to be axisymmetric, steady, turbulent and incompressible. The geometry and coordinate system are shown in figure 1. The governing equations, using time-averaged Navier-Stokes equations become:

Continuity equation:

$$\frac{\partial U_i}{\partial x_i} = 0 \qquad (1)$$

Momentum equation:

$$\rho U_j \frac{\partial U_i}{\partial x_i} = -\frac{\partial P}{\partial x_i} + \frac{\partial}{\partial x_j}\left[\mu\left(\frac{\partial U_i}{\partial x_j} + \frac{\partial U_j}{\partial x_i}\right) - \overline{\rho u_i u_j}\right] \quad (2)$$

The momentum equation contains the Reynolds stress term $-\overline{\rho u_i u_j}$; their determination requires the introduction of a turbulence model. The high-Reynolds k-ε model (*Launder and Spalding (1974)*) incorporating the Boussinesq turbulent viscosity concept to model the Reynolds stress by introducing two extra equations for the calculation of turbulent quantities is used. However, this model is not applicable in the vicinity of the solid walls in which the viscous effect is neglected. Therefore, the procedure suggested to improve numerical results, is to use separate model to treat the near wall boundary when the high-Reynolds model is used. Another procedure which we have used is to use the low Reynolds k-ε model proposed by *Launder and Sharma (1974)* (LS) instead of the high-Re model. In this case the transport equations of the turbulent kinetic energy, k, and the turbulent dissipation rate, ε, are as follows:

$$\rho U_j \frac{\partial k}{\partial x_j} = \frac{\partial}{\partial x_j}\left[\left(\mu_l + \frac{\mu_t}{\sigma_k}\right)\frac{\partial k}{\partial x_j}\right] + \mu_t\left(\frac{\partial U_i}{\partial x_j} + \frac{\partial U_j}{\partial x_i}\right)\frac{\partial U_i}{\partial x_j} - \rho\hat{\varepsilon} \quad (3)$$

$$\rho U_j \frac{\partial \varepsilon}{\partial x_j} = \frac{\partial}{\partial x_j}\left[\left(\mu_l + \frac{\mu_t}{\sigma_k}\right)\frac{\partial \varepsilon}{\partial x_j}\right] + C_1 f_1 \mu_t \frac{\varepsilon}{k}\left(\frac{\partial U_i}{\partial x_j} + \frac{\partial U_j}{\partial x_i}\right)\frac{\partial U_i}{\partial x_j} - C_2 f_2 \rho\frac{\varepsilon^2}{k} + E_\varepsilon \quad (4)$$

where $\hat{\varepsilon} = \varepsilon + D_k$ and μ_t the turbulent viscosity, which is expressed as:

$$\mu_t = \rho C_\mu f_\mu \frac{k^2}{\varepsilon}$$

In this expression, the values for turbulent constants, C_μ, f_μ were recommended by several authors.

The above steady conservation equations for any scalar variables can be written in the general form (*S. V. Patankar (1980)*):

$$\frac{\partial}{\partial x}(r\rho U\Phi) + \frac{\partial}{\partial r}(r\rho V\Phi) = \frac{\partial}{\partial x}\left(r\mu_\phi\frac{\partial \Phi}{\partial x}\right) + \frac{\partial}{\partial r}\left(r\mu_\phi\frac{\partial \Phi}{\partial r}\right) + rS_\Phi \quad (5)$$

where x and r are coordinate directions, U and V are time-averaged velocities in x and r directions respectively; μ_ϕ and S_ϕ are the turbulent diffusivity and the source term for the general scalar variable ϕ.

All the governing equations and turbulent constants used in this study are summarized in table 1 and 2.

Φ	μ_ϕ	S_ϕ
U	μ_{eff}	$-\frac{\partial P}{\partial x} + \frac{\partial}{\partial x}\left(\mu_{eff}\frac{\partial U}{\partial x}\right) + \frac{1}{r}\frac{\partial}{\partial r}\left(r\mu_{eff}\frac{\partial V}{\partial x}\right)$
V	μ_{eff}	$-\frac{\partial P}{\partial r} + \frac{\partial}{\partial x}\left(\mu_{eff}\frac{\partial U}{\partial r}\right) + \frac{1}{r}\frac{\partial}{\partial r}\left(r\mu_{eff}\frac{\partial V}{\partial r}\right) - \frac{2\mu_{eff}V}{r^2}$
k	$\mu_l + \frac{\mu_t}{\sigma_k}$	$\mu_t G - \rho\varepsilon - \mathrm{Dk}$
ε	$\mu_l + \frac{\mu_t}{\sigma_\varepsilon}$	$C_1\mu_t f_1 G\frac{\varepsilon}{k} - C_2 f_2 \rho\frac{\varepsilon^2}{k} + E_\varepsilon$

Here,

$\mu_{eff} = \mu_l + \mu_t$,

$$G = \left(\frac{\partial U}{\partial r} + \frac{\partial V}{\partial x}\right)^2 + 2\left(\frac{\partial U}{\partial x}\right)^2 + 2\left(\frac{\partial V}{\partial r}\right)^2 + 2\left(\frac{V}{r}\right)^2$$

Table 1. Conservation equations

	Standard model	Launder-Sharma
D_k	0	$2\mu_l\left(\partial\sqrt{k}/\partial x\right)^2$
E_ε	0	$2\mu_l\mu_t/\rho\left(\partial^2 V/\partial^2 x\right)^2$
f_μ	1	$\exp(-3.4/(1+R_t/50)^2)$
f_1	1	1
f_2	1	$1-0.3\exp(-R_t^2)$
C_μ	0.09	0.09
C_1	1.44	1.44
C_2	1.92	1.92
σ_k	1	1
σ_ε	1.3	1.3

Here, $R_t = \frac{\rho k^2}{\mu\varepsilon}$ the turbulent Reynolds number

Table 2. Turbulent constants

2) Boundary conditions

The boundary conditions and the configuration of the flow field studied here are shown in figure 1. In this figure, the boundary (I) is an inlet boundary through which a uniform velocity jet, Ue, which defines the Reynolds number $Re = \frac{UeD}{\nu}$, a constant turbulent kinetic energy, k_e (with a

turbulence intensity i of 0.004) and a constant dissipation rate, ε_e (with a constant length scale λ of 0.03), are specified. On the axis of symmetry (II), zero gradient values in the radial direction were assigned to all variables except the radial velocity, V, whose value was set to zero. The boundary (III) is outflow boundary where the flow is assumed to be of the parabolic type. At this boundary zero gradient values in radial direction for k and ε were applied (*Craft et al (1993)*). Boundaries (IV) and (V) are wall boundaries, where wall function formulation together with the high-Re model were used. For the LS model, the radial and axial velocity components were set to zero as well as the turbulence energy and the dissipation rate.

3) Numerical procedure

The numerical method used in the present study is based on the modified SIMPLE algorithm (*Patankar (1980)*). The governing equations are discretized using a control volume based finite difference method, with a power law scheme. The line by line method in conjunction with a tridiagonal matrix method (TDMA) was used to obtain converged solutions iteratively. The solution is considered to be converged when the mass source normalized by the largest mass flow rate across any control-volume face is less than 0.00001. All computations were made with a grid of 38x43 for axial and radial direction respectively. The grid under the jet was uniform, while a power law type grid was chosen for the rest of the domain in the radial direction. In the x direction, a power law grid was constructed from the solid walls with the finest grid near the wall. For the low-Re model, the grid distribution in the x direction ensured that the first node adjacent to the wall was in the viscous sublayer ($x^+<10$), where $x^+ = \frac{x u_\tau}{\nu}$ is the normalized distance normal to the wall and u_τ is the friction velocity.

RESULTS AND DISCUSSION

In the present work, the studied parameters are the jet Reynolds number (4000<Re<23000) and nozzle to target plate spacing (1 < H/D < 4). The flow field as predicted by the standard high-Re and LS version of low-Re k-ε models are discussed. These results are compared with the available experimental measurements where possible.

Figure 2 shows the decay of the axial centerline velocity, Uc, as a function of distance along the jet, for both computed results by the standard high-Re and low-Re LS models for Re=8500, and results obtained by others. These results were obtained numerically by *Amano (1983)* and experimentally by *Tani and Komatsu (1966)*. For this particular figure, the origin of axial distance is taken at the nozzle inlet. Referring to this figure, we note agreement within 5%, for H/D=4, between the computed data by LS model and the above results. However, the curve as predicted by the standard high-Re model is in less agreement with these results as can be observed in the same figure. Numerical results have also shown that the centerline axial velocity is constant in the zone called the potential core of the jet, then decreases rapidly to zero velocity at the stagnation point. The rapid decrease of the centerline velocity is due to the exchange of x-direction momentum into r-direction momentum in the stagnation region. For example, for H/D=4 the centerline velocity does not start to decrease from a distance of up to about 2.5 to 3 nozzle diameters from the nozzle. Over the next 1.5D distance, as the target plate is approached, the centerline velocity drops rapidly. This result appear to agree with this reported by *Gardon and Akfirat (1965)* and *Fitzgerald and Garimella (1998)*.

The effect of nozzle to target plate spacing on the normalized pressure distribution along the impingement surface for Re=8500, as predicted by the standard high-Re and LS low-Re models, is shown in figure 3. In this work, the normalized pressure is relative to the pressure at the outlet, divided by the maximum at the stagnation point. Referring to this figure, for H/D=1 and for H/D=2, the pressure at the end of the stagnation region has a minimum value, which is negative, whereas along the wall jet region the pressure increases slightly with the downstream distance to reach the pressure at the outlet. For H/D>2, this minimum has a tendency to disappear and to displace in the radial direction as obtained in the case of submerged axisymmetric impinging jet (*Amano (1983)*). We note for the curves predicted by the high-Re model, the pressure near the stagnation line is higher than that at the stagnation point, and this may be due to the use of the near wall function formulations.

Figure 4 shows the predicted streamline contours illustrating the flow patterns for Re=23000 and different H/D, using the LS low-Re model. A toroidal recirculation zone, due to the interaction between the wall jet region and the confinement surface is shown. As the aspect ratio, H/D, increases the length of the recirculation zone increases and its center is shifted radially outward. Furthermore, a growth of the wall jet region in the direction of the stream and expansion of the streamlines in the radial direction is observed, indicating a growth of the boundary layer in the wall jet region. These results agree very well with the experimental results of *Fitzgerald and Garimella (1998)* and the visualisations previously obtained by *Garimella and Rice (1995)*. For a higher aspect ratio, the recirculation zone extends to the outlet boundary, which induces an inflow at this boundary. To ensure only outflow in the outlet boundary, the location of this boundary should be sufficiently far from the axis of symmetry. *Van Heiningen (1982)* has investigated the effect of the length of the domain on the flow field and heat transfer in the planar jet. He found that the boundary does not have a significant influence on the impingement and near-jet region, which are of major concern in this study. Then, as a compromise between accuracy and computing time the length of the computational domain was chosen to be 25 times the nozzle

diameter. Note, that using the high-Re model, the streamline contour plots, show that the size of the vortex predicted by this model is smaller than that predicted by the low-Re model.

In figure 5, the radial velocity profiles as a function of radial position at several axial distances (x/D) from the impingement surface, for H/D=4 and Re=23000, using the LS model, are presented. They are normalized with the mean jet inlet velocity and compared with those obtained experimentally by *Fitzgerald and Garimella (1998)*. Very near the impingement surface, at x/D=0.02, the radial velocity exhibits a maximum value, approximately at r/D=1. The magnitude of this maximum decreases for the axial positions further away from the impingement surface and its location shifts toward the jet centerline. For x/D>0.75 and for r/D>0.75, negative velocities can be seen, illustrating the recirculation pattern in the fluid. These results are in very good agreement with those obtained experimentally and thus confirm the ability of the LS low-Re model in the prediction of the mean flow field for a confined turbulent axisymmetric jet. For the radial turbulence intensity profiles, however, the LS model under-estimates theses quantities as presented in figure 6. In fact, the numerical results near the impingement surface (for x/D=0.1) show a maximum level of turbulence which has been attributed by Fitzgerald and Garimella to the transition from laminar to turbulent boundary layer. Numerical value for this maximum is of 13.5% at r/D=2, while it is of 17.8% from measurements. This discrepancy as well as the one near the outlet section is believed to arise from the use of the jet inlet and outlet conditions respectively, in numerical calculation, the latter appears to be more important. Note that by using the LS model, *Craft et al (1993)* have obtained an over-estimation of the turbulent momentum and heat transfer rates in the stagnation region in the case of unconfined axisymmetric impinging jet. Nevertheless, our computations for both k-ε models display the same behaviour as experiment. In fact, as x/D increases the turbulence levels decrease and move radially outward as the turbulence diffuses through the boundary layer. At large x/D a second region of high turbulence can be seen to occur at r/D≈0.5. This corresponds also to an increase of the turbulent energy and is due to the high-shear layer around the free jet.

CONCLUSIONS

A numerical investigation of the application of the high-Re and low-Re (LS) number versions of k-ε models to jet impingement into parallel discs has been carried out. Results have shown very good agreements with experimental data obtained by *Fitzgerald and Garimella* , mostly on means quantities for velocity profiles. Better results are obtained with LS model. However, the radial turbulence intensity, Vrms, is under-estimated with these models. Even though these differences may be attributed to numerical grid and the used boundary conditions, most especially at the outlet section, where zero gradient in radial direction for turbulence quantities are applied, the applicability of these turbulence models in this case of this confined axisymmetric jet is still a question, as also found by *Craft et al (1993)* in the case of unconfined axisymmetric jet.

BIBLIOGRAPHY

Amano R. S., 1983, "Turbulence effect on the impinging jet," Bulletin of the JSME, vol. 26, No. 221, pp. 1891-1899.

Barata G. M. M., Durao D. F. G., and Heitor N. V., 1991, "Single and twin turbulent jets through a crossflow," *AIAA J*, vol.29, N4, pp. 595-602.

Craft T. J., Graham L. J. W. and Launder B. E., 1993, "Impinging jet studies for turbulence model assessment-II. An examination of the performance of four turbulence models," *Int. J. Heat. Mass Transfer*, vol. 36, N10, pp. 2685-2697.

Fitzgerald J. A. and Garimella S. V., 1998, "A study of the flow field of a confined and submerged impinging jet," *Int. J. Heat. Mass Transfer*, 41, pp.1025-1034.

Gardon R. and Akfirat J. C., 1965, "The role of turbulence in determining the heat transfer characteristics of impinging jets," *Int. J. Heat. Mass Transfer*, vol. 8, pp. 1261-1272.

Garimella S. V. and Rice R. A., 1995, "Confined and submerged liquid jet impingement heat transfer," *Journal of Heat Transfer*, vol. 17, pp. 871-877.

Jambunathan K., Lai E., Moss M. A. and Button B. L., 1992, "A review of heat transfer data for single circular jet impingement," *Int. J. Heat and Fluid Flow*, vol. 13, N2, pp. 106-115.

Jambunathan K. and Button B. L., 1994, "Jet impingement heat transfer: a bibliography 1976-1985," *Previews Heat Mass Transfer*, vol. 20, N5, pp. 385-413.

Launder B. E. and Spalding D. B., 1974, "The numerical computation of turbulent flows," *Comput. Methods Appl. Mech. Eng*, vol. 3, pp. 269-289.

Launder B. E. and Sharma B. I., 1974, "Application of the energy dissipation model of turbulence to the calculation of flow near a spinning disc," *Lett. Heat Mass Transfer, vol.* 1, pp. 131-138.

Patankar. S. V., 1980, Numerical Heat Transfer and Fluid Flow. McGraw-Hill, New York.

Seyedein S. H., Hasan M. and Mujumdar A. S., 1994, "Modelling of a single confined turbulent slot jet impingement using various k-ε turbulence models," *Appl. Math. Modelling*, vol. 18, pp. 526-537.

Tani I. and Komatsu Y., 1966, *Int. Congress of Appl. Mech* , pp. 672.

Van Heiningen A. R. P., 1982, "Heat transfer under an impinging slot jet," Ph.D. Thesis, McGill University.

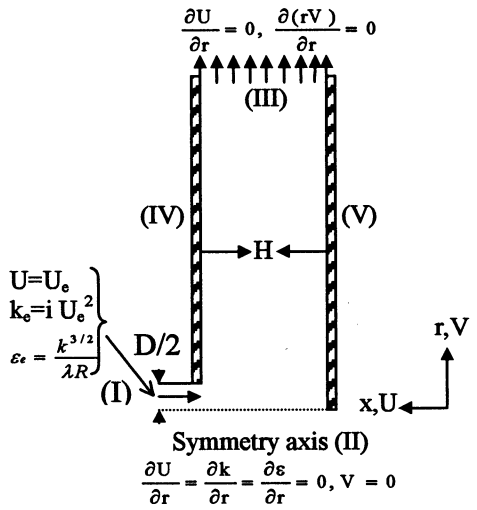

Figure 1. Configuration of flow field studied and boundary conditions.

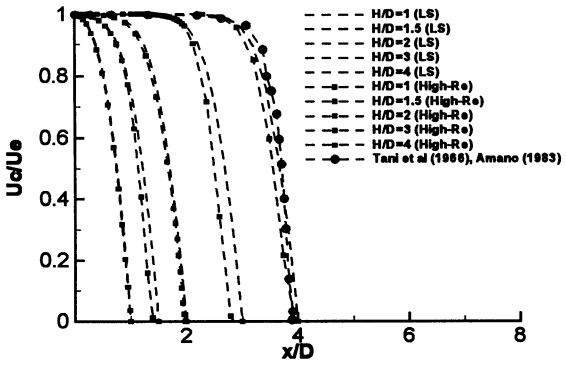

Figure 2. Effect of nozzle to target plate spacing on profile of centreline axial velocity predicted by High-Re and LS models for Re=8500.

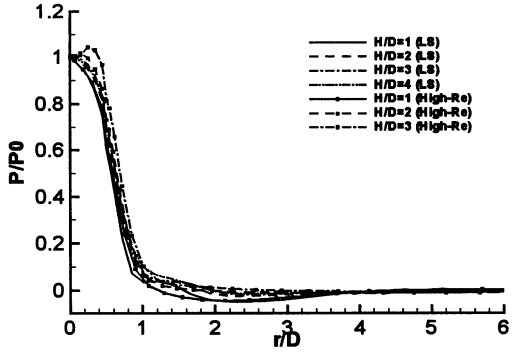

Figure 3. Normalized pressure distribution along the impingement surface for Re=8500 *and different values of H/D, predicted by High-Re and LS models.*

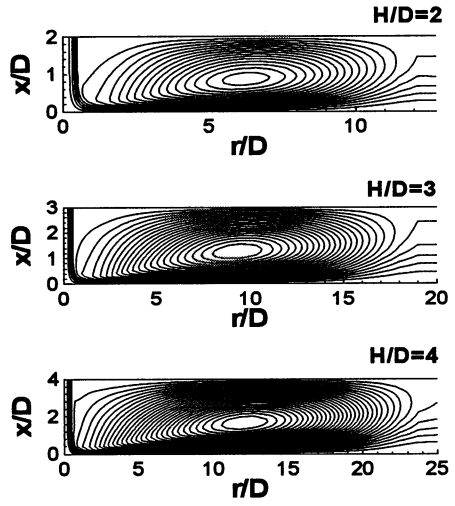

Figure 4. Streamlines illustrating the recirculating flow patterns predicted by LS model for Re=23000, for H/D=2, H/D=3 and H/D=4.

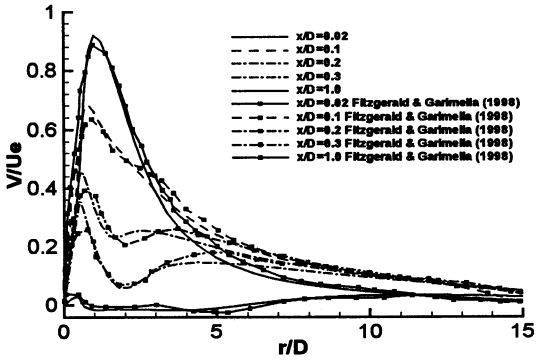

Figure 5. Comparison between predicted and experimental radial velocity profiles at different distances from the impingement surface, for H/D=4 and Re=23000.

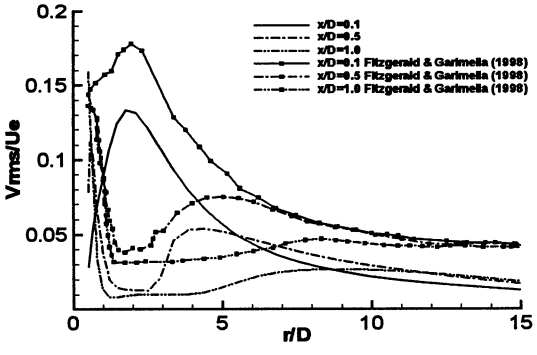

Figure 6. Comparison between predicted and experimental turbulence intensity profiles at different distances from the impingement surface, for H/D=4 and Re=23000.